


RESEARCH

Open Access



On-chip optical sources of 3D photonic integration based on active fluorescent polymer waveguide microdisks for light display application

Chunxue Wang, Daming Zhang, Jian Yue, Hang Lin, Xucheng Zhang, Tong Zhang, Changming Chen*  and Teng Fei*

*Correspondence:
chenxm@jlu.edu.cn; feiteng@jlu.edu.cn

State Key Laboratory of Integrated Optoelectronics, College of Electronic Science and Engineering, Jilin University, Changchun 130012, People's Republic of China

Abstract

In this work, on-chip three-dimensional (3D) photonic integrated optical sources based on active fluorescent polymer waveguide microdisks are proposed for light display application. Fluorescent green and red oligomers with high-efficiency photoluminescence are doped into epoxy crosslinking SU-8 polymer as the waveguide gain medium. The microdisk-based on-chip optically pumping light sources are designed and fabricated using the organic functionalized materials by direct UV written process. The promising stacking dual-microdisk structures with double gain layers could provide white signal light source generated perpendicular to the chip, and green signal light source stimulated in the chip. The approach could realize the monolithically on-chip assembled vertical and horizontal bright emitters. The optical pumping threshold power is obtained as 50 mW with continuous-wave (CW) pumping. The average gain coefficient of a white light source is measured by vertical fiber coupling as 112 dB/W, and that of green light source by horizontal fiber coupling as 137 dB/W, respectively. The rising and falling response time of the on-chip optical sources are 60 and 80 μ s under modulating pulsed pumping. This technique is very promising for achieving 3D integrated light display application, including photonic circuits and optical information encryption.

Keywords: 3D photonic integration, Active fluorescent polymers, Optical waveguide microdisks, Light display application

Introduction

As a critical component of integrated optics, planar optical waveguide chips demonstrate the ability to control and transmit optical signals well in one or two dimensions [1, 2]. Therefore, optical waveguides have been applied to various types of photonic devices, such as directional couplers, optical modulators, filter cavities, and optical display devices [3–6]. Diversified designs of optical waveguide chips have been proposed for optical display functions. Flexoelectric-effect-based light waveguide helps to realize

transparent display in liquid crystal displays (LCDs) [7]. A wedge design can be used to reduce the thickness of the optical waveguide in display function. A type of surface-relief optical waveguide display device fabricated with polycarbonate materials was realized [8]. However, the integration and miniaturization of photonic chips depending on the traditional planar lightwave circuits (PLC) with single-layer two-dimensional (2D) optical waveguide structure have been significantly limited. Compared with 2D photonic integrated model, three-dimensional (3D) monolithically optical integrated circuits possess more flexible spatial extensibility and more diverse functional integration selectivity, which are playing a key role for high-integration and mini-size optical display modules [9, 10]. The 3D multilayer stacking optical waveguide integrated technique could relieve more stress on footprint of photonic chips and provide more sufficient space for multilayer optical display [11–13]. Meanwhile, the 3D on-chip photonic integrated module could realize a high versatility and compatibility for various key elements of light generation, processing, modulation, and detection on the same photonic platform [14, 15]. Specially, the 3D on-chip integrated optical sources based on micro-nano optically or electrically pumping light-emitting devices (LEDs) are critical parts for 3D on-chip photonic integrated technology, which is vital to build 3D spatial optical display systems [16, 17]. Considering LEDs with the role of light display application, which may provide a new idea for achieving functional-oriented 3D on-chip integrated optical sources [18].

On-chip integrated photonic devices based on polymer waveguide materials can simultaneously possess various advantages. i) The polymer material system is easy to be doped with chromophores, so the active multi-functional optical polymer waveguide structure can be directly achieved [19]. ii) Compared with inorganic photonic platform, the polymer integrated waveguide fabrication process is simple and low cost [20]. iii) In particular, the polymer-based photonic platform is more suitable for achieving on-chip multilayer stacking structure using only spin-coating process, without complicated epitaxial growing steps for waveguide thin film [21, 22]. Due to the high flexibility and manufacturability of polymer waveguide chips, their fabrication techniques have been applied to realize LEDs light source and projection display facilities [23, 24]. Contrast to traditional inorganic semiconductor materials, such as silicon, InP and GaAs, functionalized organic polymers as main raw for on-chip optical system have been reported to achieve typical passive, dynamic and active high-performance optical waveguide chips, such as gratings, thermo- or electro-optic modulators/switches, and amplifiers [25–28]. Furthermore, waveguide-typed organic light-emitting devices (OLEDs) based on functionalized polymers have been also used as optical sources and light displays in daily life [29, 30]. The polymer-based integrated photonic platform adapted for 3D fabrication method for on-chip multi-functional integration with both OLEDs and polymer waveguide circuits, with no extra wafer-bonding or flip-chip bonding process for optical source parts [31, 32].

In this work, on-chip 3D photonic integrated optical sources based on active fluorescent polymer waveguide microdisks are first proposed to light display application. The UV–Vis optical absorption and photoluminescence characteristics of fluorene-based two chromophores are analyzed. As green (TCBzC) and red (TCNzC) emissive oligomers, TCBzC and TCNzC are doped into epoxy SU-8 polymer to form a waveguide gain medium. The active waveguide microdisk structure for on-chip optically pumping light

source is optimally designed and the waveguide device is fabricated by the direct UV written process. The properties of monolithically on-chip assembled vertical and horizontal bright emitters based on single-microdisk resonator are researched. The stacking dual-microdisk architecture with double gain layers is given subsequently, which could provide white signal light source emitted perpendicular to the chip, and green signal light source stimulated in the chip. The gain properties under CW pumping and frequency response features under modulated pulsed pumping for dual-microdisk optical sources are measured, respectively. This technique is potential for photonic integrated circuits, light displays, and optical information encryption etc.

Materials and methods

Fluorescent gain polymer waveguide materials

As illustrated in Fig. 1a, fluorene-based chromophores TCBzC and TCNzC were synthesized as green and red emissive materials [33, 34]. TCBzC and TCNzC are composed of four alkyl-linked peripheral carbazole groups and an emissive rigid core. Alkyl-linked peripheral carbazole groups and emissive rigid core were used as electron-donating and electron-withdrawing units. Green- and red-light emissions were achieved by through different emissive rigid cores (2,1,3-benzothiadiazole for TCBzC and 2,1,3-naphthothiadiazole for TCNzC). The 5 wt% TCBzC and TCNzC with high photo-luminescence (PL) efficiency were doped in epoxy crosslinking SU-8 polymer to form the gain medium. The TCBzC/SU-8 and TCNzC/SU-8 could form transparent and homogeneous solutions as shown in Fig. 1a, which can generate PL phenomenon under the stimulant light. The optical absorbance and PL spectra of TCBzC and TCNzC are given in Fig. 1b. It could be observed that the PL emission peak wavelengths as 540 nm (green) and 611 nm (red) are obtained for TCBzC and TCNzC with the excitation of 365 nm wavelength, respectively. The flexible alkyl linking molecular structures of the emissive oligomers could endow promising solubility and dispersibility, and the compact epoxy crosslinking network of SU-8 could guarantee relatively high thermal stability. Moreover, as shown in Fig. 1c,

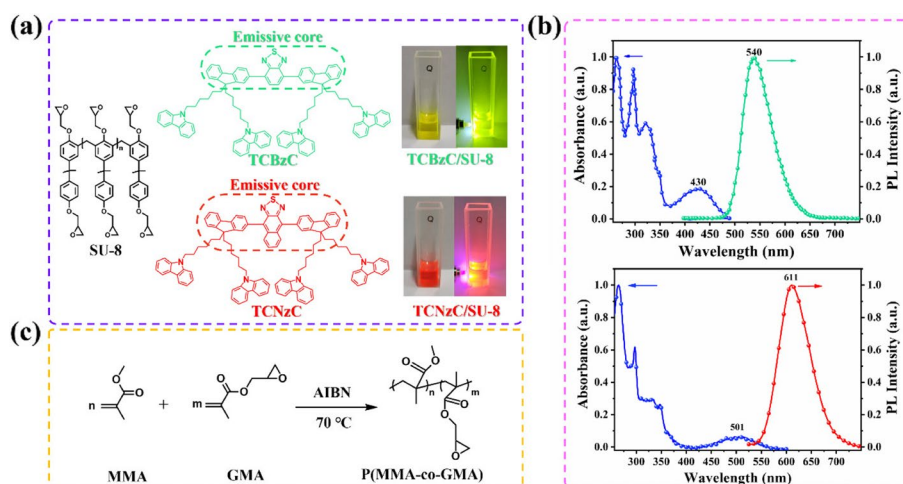


Fig. 1 **a** Molecular structures of SU-8, TCBzC, and TCNzC. The transparent TCBzC/SU-8 and TCNzC/SU-8 solution as the waveguide gain medium; **b** optical absorbance and PL spectra of TCBzC and TCNzC, respectively; **c** the synthesis process of P(MMA-co-GMA) cover cladding material

copolymer of methyl methacrylate (MMA) and glycidyl methacrylate (GMA), P(MMA-co-GMA) was self-synthesized as cover cladding material (the synthesis process can be found in the [Supplementary Material](#)). The root-mean-square (RMS) surface roughness of gain polymer and P(MMA-co-GMA) thin films were measured less than 0.5 nm, which were advantageous for achieving high-quality waveguide devices [35]. High transparency of P(MMA-co-GMA) in the visible band was beneficial to realize low-loss waveguide device. In an actual experiment, SU-8 polymers doped with 5 wt% TCBzC and TCNzC were utilized as the gain waveguide materials. The refractive indices of gain polymer and P(MMA-co-GMA) thin films were measured as 1.585 and 1.490, respectively. Due to the low doping concentration of emissive oligomers, the refractive index (RI) of gain material was similar for TCBzC and TCNzC.

Design and simulation of 3D photonic integrated optical sources

As shown in Fig. 2a and b, the schematic architecture and operating principle of microdisk-based on-chip optically pumping light sources compatible with both vertical and horizontal emitting directions were described using the fluorescent gain polymer waveguide structure. As given in Fig. 2c, the schematic cross-sectional profile of the waveguide structure was exhibited. The thickness of P(MMA-co-GMA) cover cladding and SiO₂ buffer layer (RI @ 1.46) was defined as 8 and 5 μm, respectively. The width and height for the core waveguide were set as 7 and 5 μm, respectively.

The output optical power intensity for the multimode interference (MMI) power distributor with different lengths of interference region was given in Fig. 3a. It can be found that when 405 nm wavelength pumping light was loaded into the bus waveguide with the interference region length of the MMI power distributor as 40 μm, 75% of the light power was coupled into microdisk, and 25% was transmitted straightly into *Add* channel by the MMI power distributor shown in Fig. 3b. Pumping light will be resonated in the microdisk cavity and absorbed by gain medium, which will stimulate fluorescent optical source perpendicular to the chip. Meanwhile, nearly 20% of pumping light in the microdisk will be coupled into *Drop* channel by symmetrical MMI power distributor. The pumping light in *Add* and *Drop* channels will also excite

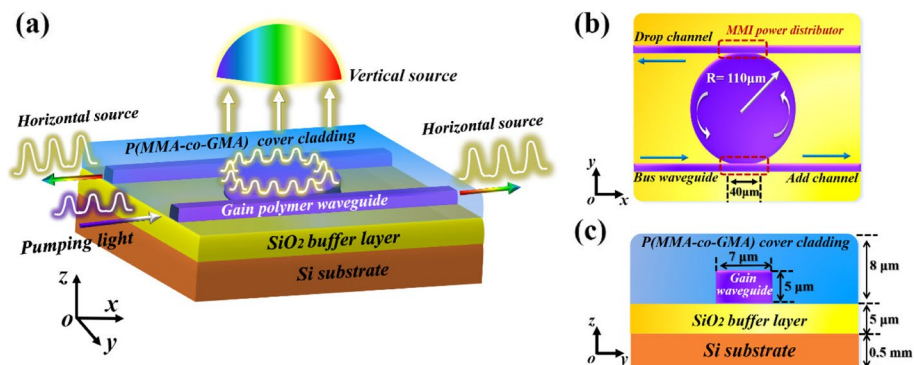


Fig. 2 Schematic diagram of the 3D photonic integrated optical sources. **a** The schematic architecture and operating principle of the microdisk-based on-chip optically pumping light sources; **b** structural parameters of the microdisk-based waveguide resonator in x - y profiles; **c** the size of cross-sectional gain waveguide in y - z profiles

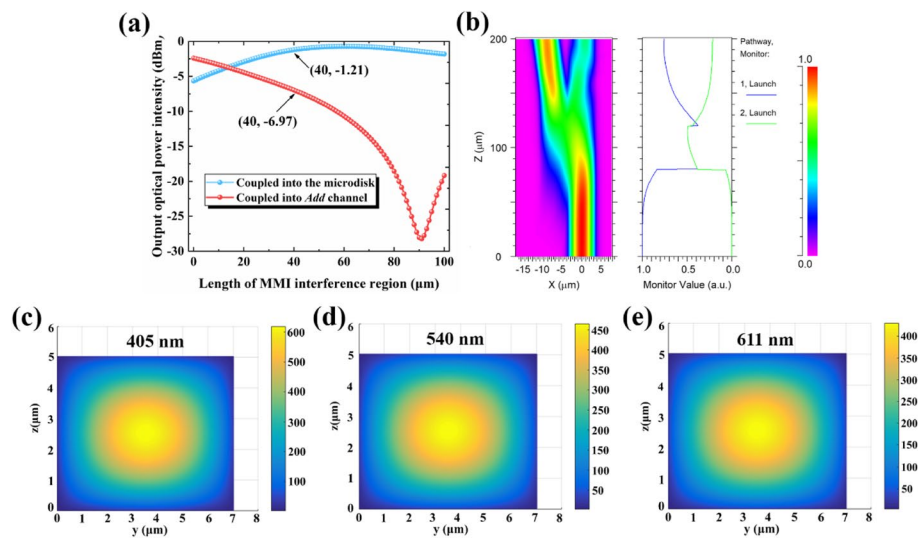


Fig. 3 The design of the MMI power distributor and calculation results of optical field modes in waveguide core layers at different wavelengths. **a** The output optical power intensity at different interference region lengths; **b** optical field distribution on the x-y plane; **c**, **d**, and **e** were the cross-sectional optical field distributions of fundamental mode in waveguide core layer at 405, 540, and 611 nm wavelength, respectively

bi-directional fluorescent optical sources in the chip. Through this approach, the monolithically on-chip assembled vertical and horizontal bright emitters will achieve 3D integrated light sources. And in Fig. 3c, d, and e, the optical field distributions of fundamental mode in gain waveguide for 405 nm pumping light, for 540 nm green stimulated light, and for 611 nm red stimulated light were simulated, respectively. It could be obtained that the fundamental-mode overlapping integral factor (Γ) between pumping and stimulated light was calculated to be 99.99%, which was beneficial for enhancing the emission efficiency.

The microdisk-based cavity with the resonant wavelength as 405 nm was designed and optimized as given in Fig. 4. The relationship between the resonant wavelength and free spectral range (FSR) of the waveguide microdisk resonator with various radii was shown in Fig. 4a. It can be concluded from that when the radius of the microdisk was increased, the FSR of the waveguide resonator will be reduced. The resonant wavelength of the microdisk can be defined as 405 nm corresponding to 110 μm of the radius. Figure 4b showed the relationship between microdisk resonator radii and the optical power intensity with different waveguide core layer thickness. It can be obtained that when the radius was 110 μm and the core thickness was 5 μm, the bending loss of the microdisk will be low. Therefore, the radius of the microdisk and the thickness of the waveguide core layer were set as 110 and 5 μm, respectively. The value of FSR was obtained as 0.14 nm. As given in Fig. 4c, the optical transmission spectrum of the microdisk-based resonator was calculated. It could be obtained that the quality factor (Q) is 9.185×10^5 at 405 nm resonance peak wavelength. According to the parameters of the waveguide structure, optical transmission field of the waveguide microdisk resonator designed corresponding to 405 nm wavelength pumping light was simulated by finite-difference time-domain (FDTD) solution as illustrated in Fig. 4d. It was observed that optical resonance was enhanced through whispering-gallery-mode microdisk-based cavity and the

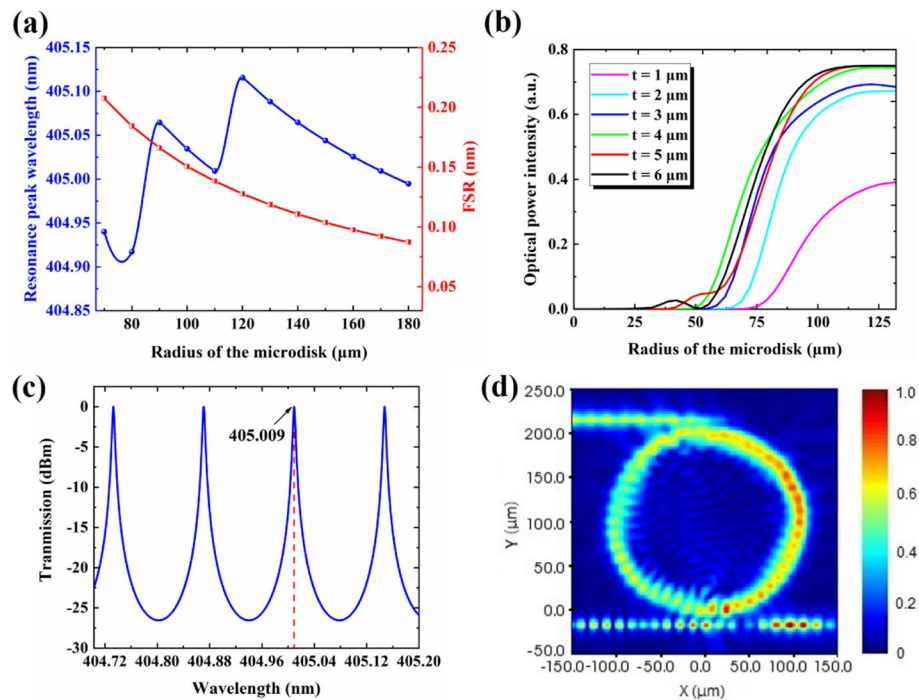


Fig. 4 Optical properties simulation analysis of the designed waveguide microdisk-based resonator. **a** The calculation results of resonance wavelength and FSR with different microdisk radii; **b** relationship between microdisk resonator radii and the optical power intensity with different waveguide core layer thickness; **c** the optical transmission spectrum of the microdisk-based resonator; **d** optical transmission simulation of the waveguide microdisk resonator

pumping light identical to the setting proportion was coupled into *Add* and *Drop* channels by MMI power distributors.

Results and discussion

Fabrication and testing of single-microdisk optical sources

The actual microdisk-based on-chip optically pumping light sources were fabricated using the fluorescent polymer waveguide materials by direct UV written process (Figures S1a-1e, [Supplementary Material](#)). As shown in Fig. 5a, the top-view entire waveguide structure of the single-microdisk 3D integrated optical source was measured by an optical microscope ($\times 100$) and the cross-sectional waveguide image was obtained by scanning electron microscope (SEM), respectively. It could be found that the size of the waveguide device had been achieved very well. The 3D integrated single-microdisk optical sources excited by 405 nm wavelength pumping light were measured through horizontal and vertical fiber coupling technique. The titling angle of vertical cavity-fiber coupling was 8° , which was beneficial to improve the coupling efficiency. The measuring images captured by the CCD camera were given in Fig. 5b and c, respectively. It could be observed that the pumping light was coupled into bus waveguide by horizontal input fiber and the fluorescence generated from microdisk cavity were coupled into the vertical output fiber. The propagation loss and facet coupling loss of the straight waveguide were measured by the cut-back method in (Figure S3, [Supplementary Material](#)).

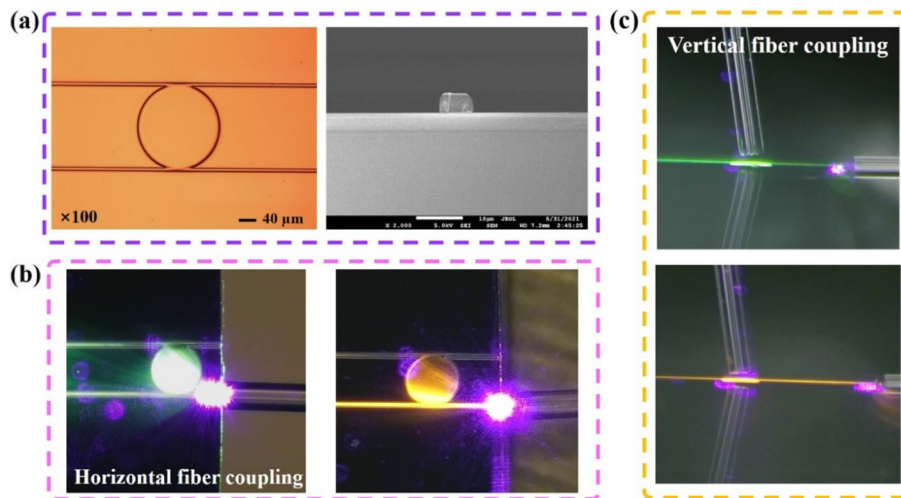


Fig. 5 Structural size of the waveguide structure and the horizontal and vertical fiber coupling of 3D integrated single-microdisk optical sources excited by 405 nm wavelength pumping light. **a** The top-view (optical microscope) and cross-sectional view (SEM image) of the gain waveguide structure; **b** and **c** were the images of horizontal fiber coupling for inputting pumping light and vertical fiber coupling for outputting fluorescence, respectively

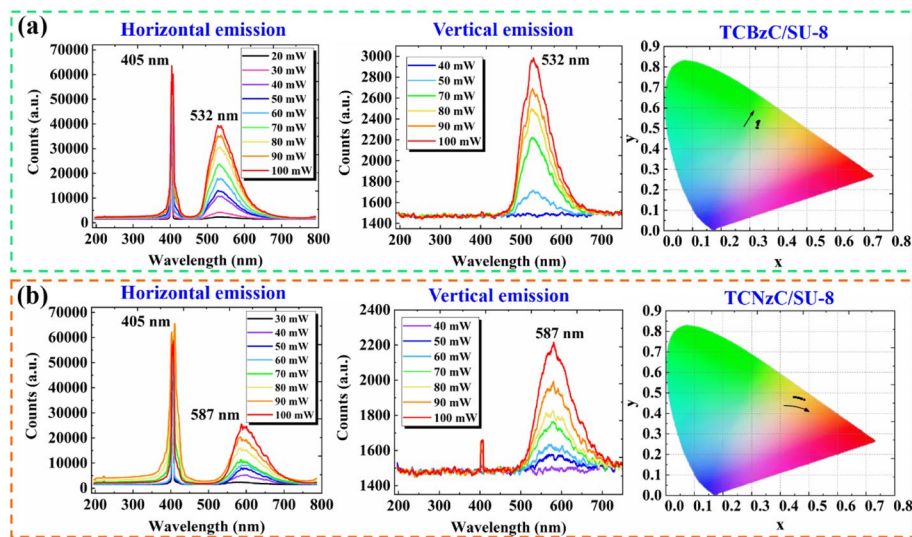


Fig. 6 a Horizontal and vertical output optical spectra for the microdisk-based 3D integrated bright sources for TCBzC/SU-8, and the corresponding CIE chromaticity diagram coordinates of the fluorescent light; **b** horizontal and vertical output spectra for the microdisk-based 3D integrated on-chip optical sources for TCNzC/SU-8, and the corresponding CIE chromaticity diagram coordinates of the fluorescent light

As shown in Fig. 6a and b, the horizontal and vertical output optical spectra for the microdisk-based 3D integrated optical sources were analyzed by the visible light spectrometer (Shanghai, Fuxiang Optics) measuring system. When the optical power of pumping light increased from 40 to 100 mW, the optical intensity of 3D on-chip sources enhances gradually. The CIE chromaticity diagram coordinates of the output light were collected, from (0.3258, 0.5302) to (0.3332, 0.5351) as green light corresponds to TCBzC/SU-8, and from (0.4623, 0.4760) to (0.4847, 0.4662) as orange light

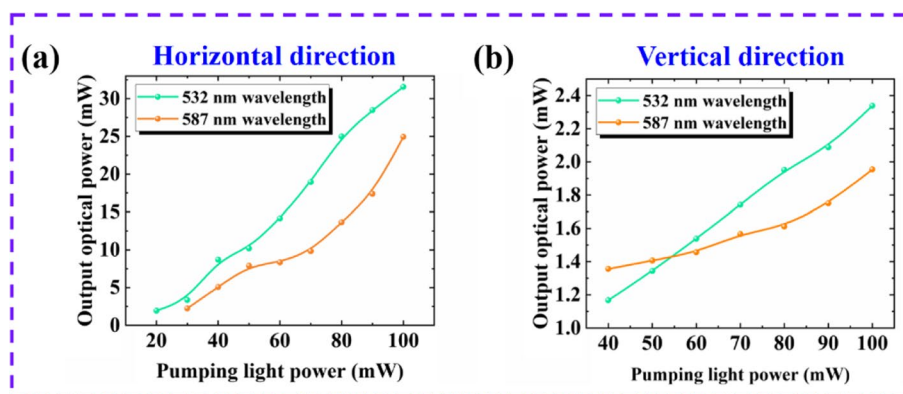


Fig. 7 The output power of both **a** horizontal and **b** vertical emissions for single-microdisk light source at 405 nm pumping light

Table 1 The horizontal and vertical average gains based on the active polymers for the 3D integrated on-chip optical sources

FGPM	ODAS	PLW (nm)	EPW (nm)	Pumping light power (mW)									
				30	40	50	60	70	80	90	100		
				Average gain (dB)									
TCBzC/SU-8	HE	405	532	2.20	4.42	7.36	8.52	9.95	10.70	11.13	11.79		
TCNzC/SU-8	HE	405	587	/	3.32	5.43	5.96	6.82	8.41	9.21	10.36		
TCBzC/SU-8	VE	405	532	/	/	/	0.66	1.74	2.23	2.74	3.30		
TCNzC/SU-8	VE	405	587	/	/	0.15	0.31	0.63	0.75	1.11	1.69		

FGPM Fluorene-based gain polymer material, ODOS Output direction of optical sources, PLW Pumping light wavelength, EPW Emission peak wavelength, HE Horizontal emission, VE Vertical emission

was related to TCNzC/SU-8 in Fig. 6a and b, respectively. For the CIE coordinates of green and orange light sources, the calculated results of the color difference ranges were 2.4% and 3.8%, respectively. Meanwhile, it could be obtained that the actual emitting peak wavelength for microdisk-based bright sources using TCNzC/SU-8 as the gain polymer waveguide material is 587 nm. Compared with original 611 nm wavelength emission of pure TCNzC chromophore, the hypsochromic shift (24 nm) is attributed to the reduced aggregation of TCNzC molecules in the SU-8 photoresist. The polarity of the SU-8 photoresist is weak, which is conducive to a good dispersibility of TCBzC and TCNzC in the polymer. After doping into SU-8 photoresist, the fluorescent molecules were well dispersed, and the luminescence center quenching was reduced.

And when the pumping light of 405 nm wavelength was coupled into the waveguide, the overall energy conversion efficiency were 33.8% and 26.9% for the microdisk-based TCBzC/SU-8 and TCNzC/SU-8 waveguide as shown in Fig. 7a and b, respectively.

With the excitation of 405 nm wavelength pumping light in, the TCBzC/SU-8 and TCNzC/SU-8 waveguide generated 532 nm and 587 nm peak wavelength emission light, respectively. The horizontal and vertical average gains based on data from

Fig. 6a and b for the 3D integrated on-chip optical sources were summarized in Table 1. The gains of the output optical spectra can be obtained at 50 mW pumping light threshold power. Therefore, the average gain can be calculated by the amplification ratio of the output optical spectrum intensity applied at an applied pumping light power to the optical spectrum intensity obtained at the threshold excitation by Eq. 1,

$$\text{average gain (dB)} = 10 \lg (P(s)/P(0)) \quad (1)$$

where $P(0)$ is the intensity of the initially spontaneous spectrum and $P(s)$ is the output spectrum power intensity obtained by increasing the pumping light power [36]. Thereby, the average relative gain can be defined as the maximum gain value of the waveguide chip. The average gain coefficient is the linear fitting results calculated by the relationship between the average gain of the waveguide and the value of pumping light power. Consequently, the average gain coefficients for TCBzC/SU-8 and TCNzC/SU-8 are measured as 137 and 117 dB/W for horizontal optical sources, and as 66 and 31 dB/W for vertical optical sources, respectively. In addition, it can be found from Table 1 that TCBzC/SU-8 waveguide would generate larger average gain compared with TCNzC/SU-8 waveguide in horizontal and vertical directions when the 405 nm pumping optical power is equal. This is mainly because TCBzC/SU-8 waveguide has higher absorption and power conversion efficiency of 405 nm pumping light source.

Fabrication and testing of dual-microdisk on-chip optical sources

In the following experiments, we selected 532 nm and 405 nm wavelengths as pumping light to measure the average gain of the TCNzC/SU-8 waveguide, respectively. Under the same pumping optical power, the average gain value of orange light excited by 532 nm wavelength pumping light was larger than that stimulated by 405 nm wavelength for active TCNzC/SU-8 waveguide material. As given in Fig. 8a and b, the actual measuring image of the TCNzC/SU-8 gain waveguide pumped by 532 nm wavelength was given and the CIE chromaticity diagram coordinates changed from

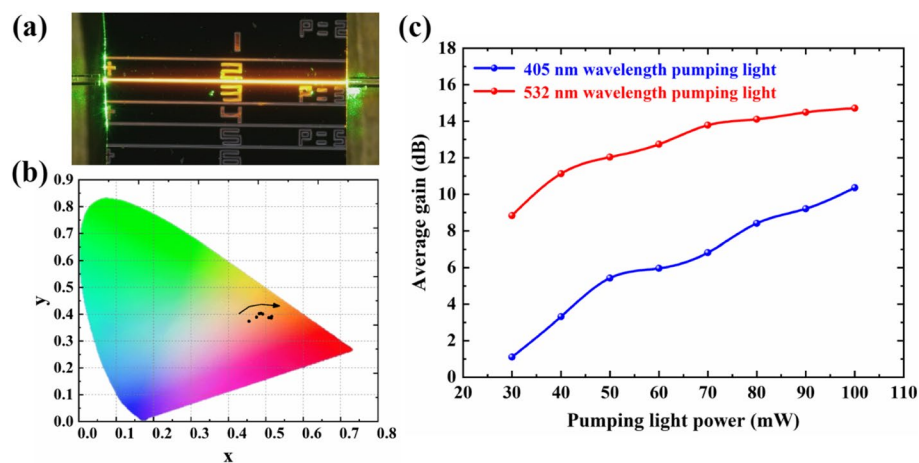


Fig. 8 **a** Image of active TCNzC/SU-8 waveguide excited by 532 nm wavelength pumping light; **b** the CIE chromaticity diagram coordinates of the spontaneous light; **c** comparison between the average gain values at 405 nm and those that at 532 nm wavelength pumping light from the output spectra

(0.4754, 0.3892) to (0.5149, 0.3853) of orange light were obtained. As given in Fig. 8c, compared with those pumped by 405 nm wavelength light, the average relative gains by 532 nm wavelength light increase ~ 7 dB at same pumping light power. The main reason is that the TCNzC has 20 times greater absorption coefficient at 532 nm wavelength than that of 405 nm wavelength based on Lambert–Beer’s law [37]. Although photon energy at 405 nm wavelength is higher than that at 532 nm wavelength, the absorption coefficient of TCNzC is much stronger at 532 nm, therefore a functional dual-microdisk waveguide chip is proposed to achieve 3D integrated light display application.

Based on above characteristics, the stacking dual-microdisk waveguide structures with double gain layers are proposed for light display application. The schematic model of dual-microdisk 3D integrated on-chip optical sources was shown in Fig. 9a. The bottom-microdisk resonator was formed by active TCBzC/SU-8 and stimulated by 405 nm wavelength pumping light. The vertical-emission green bright source from bottom-microdisk cavity was utilized as next pumping light and the horizontal-emission ones stimulated from *Add* and *Drop* channels was used as signal light in the chip. Then the vertical-emission orange bright source was generated from top-microdisk structure based on active TCNzC/SU-8 by bottom pumping light. The stimulated hybrid lights will further form white vertical-emission optical source using stacking dual-microdisk structures by energy-transfer pumping mechanism. As given in Fig. 9b and c, the radius and thickness of the top waveguide microdisk were defined as 55 and 5 μm , respectively. The gap between the top and bottom microdisks was set as 3 μm . The specific fabrication process of the actual device was described in (Figures S1a–1i, [Supplementary Material](#)).

As shown in Fig. 10a and b, green (bottom layer) and orange (top layer) fluorescent dual-microdisk waveguide chip was stimulated by a 365 nm UV point light source.

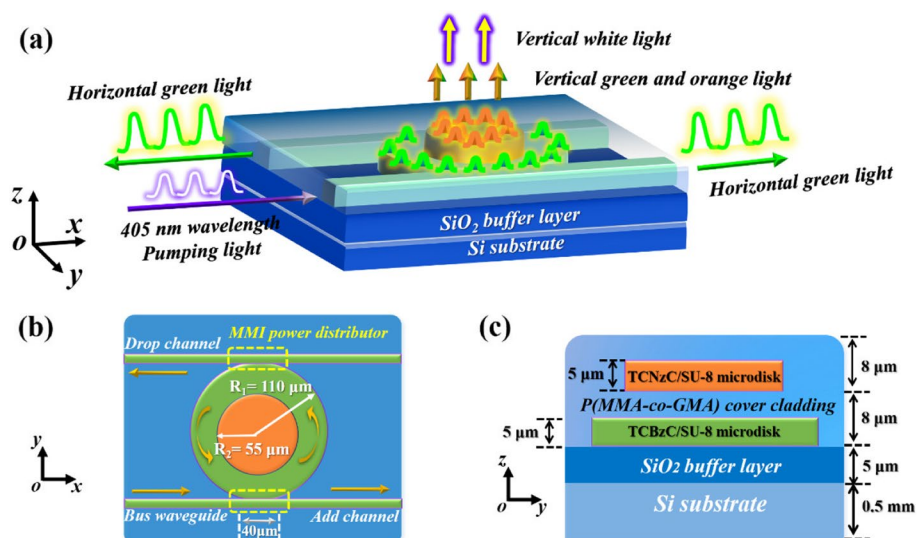


Fig. 9 **a** Schematic model of dual-microdisk 3D integrated on-chip optical sources; **b** structural parameters of the dual-microdisk waveguide devices in x – y profiles; **c** cross-sectional sizes of the top and bottom waveguide microdisks in y – z profiles

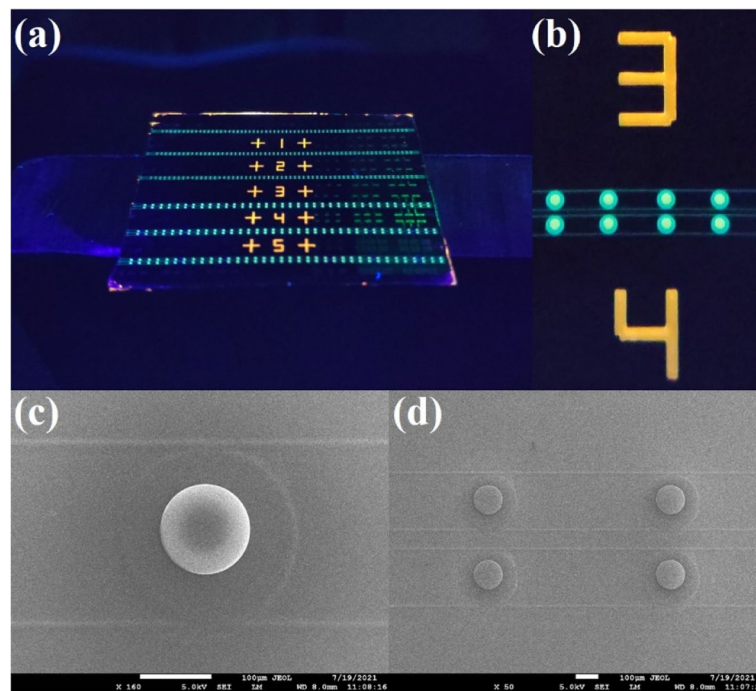


Fig. 10 **a** The actual fluorescence dual-microdisk stimulated by a UV point light source at 365 nm wavelength; **b** the images captured of white light emission for dual-microdisk chip; **c** and **d** SEM images of the dual-microdisk waveguide structures

The white light emission could be observed clearly. The SEM images of dual-microdisk structures were shown in Fig. 10c and d. It can be found that the waveguide size of the dual-microdisk device has been realized very well.

The measurements for actual dual-microdisk waveguide chip were shown in Fig. 11. The hybrid green and orange light will form white bright source. The output optical spectra of the dual-microdisk waveguide were given in Fig. 11a and b, respectively. As illustrated in Fig. 11c, with the increasing of pumping light power, the CIE coordinate moved from (0.4247, 0.3533) to (0.3472, 0.3127). For the white light source waveguide device, the CIE coordinates shift of the white light emission is a little greater, mainly for when the 405 nm pumping light power increases, the power of the green light generated in the TCBzC/SU-8 waveguide will reach the threshold of the orange light in TCNzC/SU-8 waveguide, and the orange light power of the upper waveguide increases. When the power of the orange light is increased and superimposed on the green light, the CIE coordinates received gradually move from the orange zone to the white zone. The color rendering index (CRI) value of the white light is 83 and the correlated color temperature (CCT) value is 4750 K when the pumping light power is 100 mW, respectively. And was observed that vertical-emission green source stimulated by 405 nm pumping light from bottom-microdisk cavity could form vertical-emission orange optical source from top-microdisk structure as given in Fig. 11d. And with the increasing of the pumping light power, the white light source was generated.

For the dual-microdisk waveguide chip, the overall energy conversion efficiency was 33.6% according to Fig. 11a and b, as given in Fig. 12a. The curve of average gain for

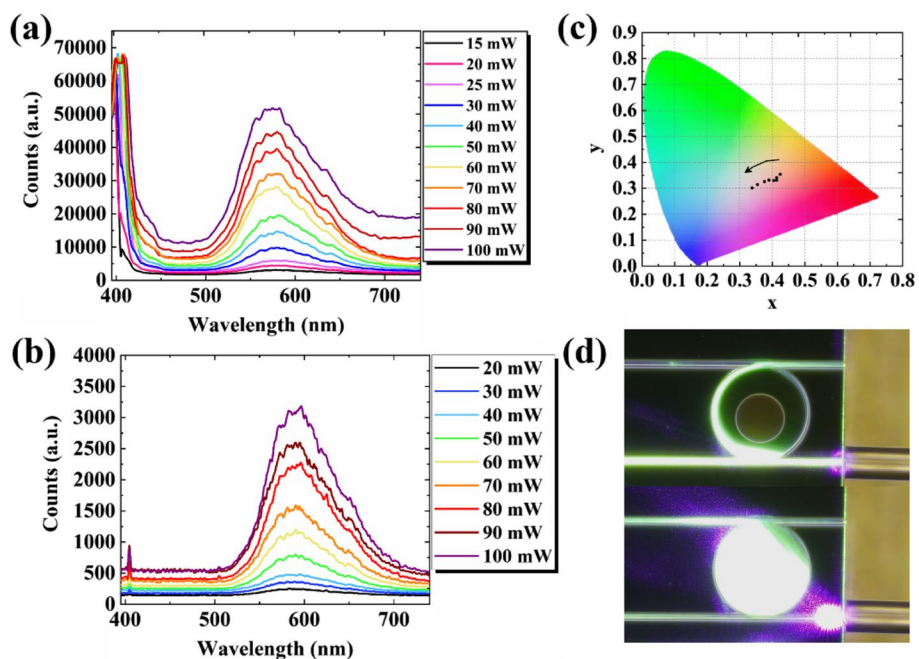


Fig. 11 The measurements for actual dual-microdisk waveguide. **a** Horizontal emission output spectra of the dual-microdisk waveguide; **b** vertical emission output spectra of the dual-microdisk waveguide; **c** the CIE chromaticity diagram coordinates of the spontaneous light; **d** the measuring images for actual dual-microdisk waveguide chip

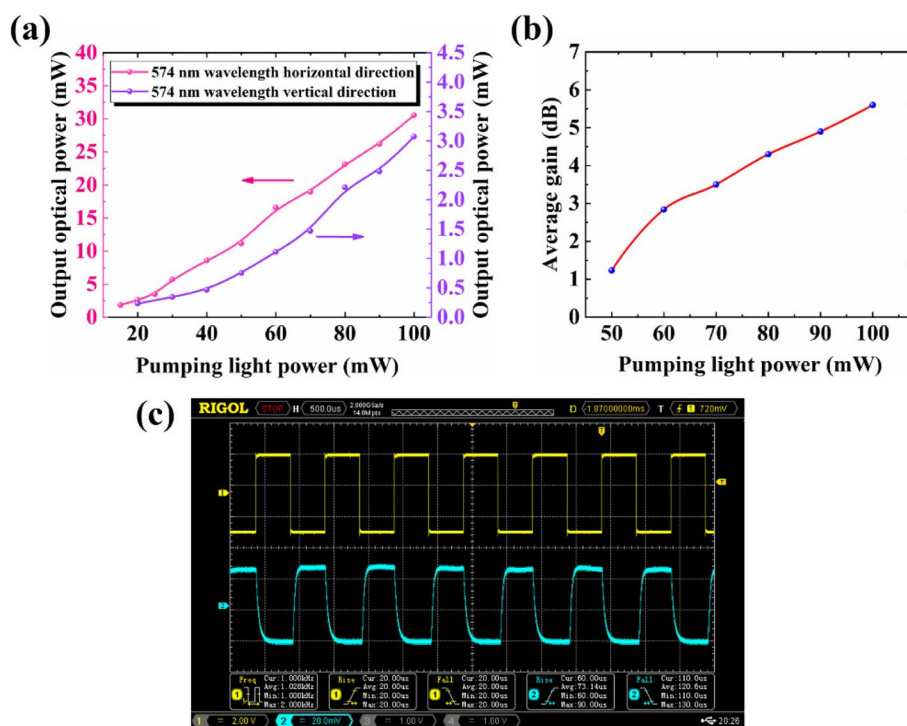


Fig. 12 **a** Optical power output for dual-microdisk waveguide; **b** the average gain of white bright source versus CW pumping light power; **c** the frequency response of white bright source under modulating pulsed optically pumping

dual-microdisk vertical-emission white source with changing pumping light power was measured as Fig. 12b. It can be found that the optical pumping threshold power was ~ 50 mW with continuous-wave (CW) pumping. When the pumping light power increased to 100 mW, the average relative gain could reach 5.6 dB. The average gain coefficient of white light source was measured by vertical fiber coupling as 112 dB/W, and that of green light source by horizontal fiber coupling as 137 dB/W, respectively. And as shown in Fig. 12c, the frequency response characteristics of white bright source were analyzed. The rising and falling response time of the vertical white light were measured as 60 and 80 μ s under modulating pulsed optically pumping with 1 kHz square electrical controlling signal, which are potential in light display technique. The detailed measuring system for CW and pulsed pumping of the chip was supplied in (Figure S2, [Supplementary Material](#)).

The long-term stability of the device was given in (Figure S4, [Supplementary Material](#)), the horizontal and vertical output optical intensity of the waveguide device still has a high fluorescence intensity in repeated experiments, and the fluorescence emission does not attenuate significantly. This high-stability photonic chip can achieve 3D integrated optical display function, which has a superior application prospect in light display application.

Conclusion

In summary, 3D photonic integrated on-chip optical sources based on active fluorescent polymer waveguide microdisks are first proposed to light display application. As green and red emissive oligomers, TCBzC and TCNzC are doped into epoxy SU-8 to form a waveguide gain medium. The microdisk-based on-chip optically pumping bright sources are designed and fabricated using the organic functionalized materials by direct UV written process. The stacking dual-microdisk structures with double gain layers could provide white signal light source generated perpendicular to the chip, and green signal light source stimulated in the chip. The average gain properties of the 3D photonic integrated on-chip optical sources with CW pumping light power are analyzed. The frequency response of the white bright source is measured under modulating pulsed pumping light. This technique is potential in light display application and optical information encryption.

Abbreviations

2D	Two-dimensional
3D	Three-dimensional
CCD	Charge coupled device
CCT	Corelated color temperature
CIE	Coherent infrared energy
CRI	Color rendering index
CW	Continuous-wave
EPW	Emission peak wavelength
FDTD	Finite-difference timedomain
FGPM	Fluorene-based gain polymer material
FSR	Free spectral range
GMA	Glycidyl methacrylate
HE	Horizontal emission
LCDs	Liquid crystal displays
LEDs	Light-emitting devices
MMA	Methyl methacrylate
MMI	Multimode interference

ODOS	Output direction of optical sources
OLEDs	Organic light-emitting devices
PL	Photo-luminescence
PLC	Planar lightwave circuits
PLW	Pumping light wavelength
RI	Refractive index
RMS	Root-mean-square
SEM	Scanning electron microscope
VE	Vertical emission

Supplementary Information

The online version contains supplementary material available at <https://doi.org/10.1186/s43074-023-00090-8>.

Additional file 1: Supplementary Material. Figure S1. The fabrication process of the waveguide dual-microdisk waveguide chip. **Figure S2.** CW pumping light and pulsed pumping light test system. **Figure S3.** The propagation loss and facet coupling loss of the straight waveguide by the cut-back method. (a) The undoped, TCBzC/SU-8, and TCNzC/SU-8 waveguides at 405 nm wavelength; (b) the undoped and TCNzC/SU-8 doped waveguides. **Figure S4.** Fluorescence emission long-term stability measurement of the waveguide chip. (a) The horizontal and vertical output optical intensity of the TCBzC/SU-8 waveguide; (b) the horizontal and vertical output optical intensity of the TCNzC/SU-8 waveguide.

Acknowledgements

Tledslede authors would like to thank Prof. Teng Fei and Prof. Tong Zhang. They provided valuable help with the synthesis of fluorene-based chromophores TCBzC and TCNzC.

Authors' contributions

C.W. and C.C. designed this work and completed the experiments; T.F. and T.Z. synthesized the materials and drew the figures; D.Z. assisted in lighting experiments with J.Y., H. L., and Z.W.; C.W. and X.Z. wrote the paper; all authors participated in the analysis of experimental data and discussion of the results. The author(s) read and approved the final manuscript.

Funding

National Key Research and Development (R&D) Program of China (2019YFB2203001) and National Natural Science Foundation of China (NSFC, No. 62171195).

Availability of data and materials

The datasets analyzed during the current study are available from the corresponding author on reasonable request.

Declarations

Competing interests

The authors declare that they have no competing interests.

Received: 13 October 2022 Revised: 23 February 2023 Accepted: 20 March 2023

Published online: 24 March 2023

References

- Kim JH, Aghaeimeibodi S, Carolan J, Englund D, Waks E. *Optica*. 2020;7:291.
- Lenzini F, Janousek J, Thearle O, Villa M, Haylock B, Kasture S, Cui L, Phan H, Dao D, Yonezawa H, Lam P, Huntington EH, Lobino M. *Sci Adv*. 2018;4:eaat9331.
- Petra R, Oo S, Tarazona A, Cernansky R, Reynolds S. *Opt Express*. 2019;27:15735.
- Schuler S, Muench JE, Ruocco A, Balci O, van Thourhout D, Soriano V, Romagnoli M, Watanabe K, Taniguchi T, Goykhman I, Ferrari AC, Mueller T. *Nat Commun*. 2021;12:3733.
- Shi A, Yan B, Ge R, Xie J, Peng Y, Li H, Sha WEI, Liu J. *Opt Lett*. 2021;46:1089.
- Cheon BJ, Kim JW, Oh MC. *Opt Express*. 2013;21:4734.
- Shin Y, Jiang Y, Wang Q, Zhou Z, Qin G, Yang D. *Photonics Res*. 2022;10:407.
- Zhang W, Wang Z, Xu J. *Appl Opt*. 2018;57:3720.
- Park J, Joo J, Kwack M, Kim G, Han SP, Kim S. *Opt Express*. 2021;29:35261.
- Bamiedakis N, McKendry J, Xie E, Gu E, Dawson M, Penty R, White IH. *J Lightw Technol*. 2019;37:3305.
- Sun C, Gao Z, Teng K, Niu L, Chen Y, Zhao Y, Yang Q. *Appl ACS Mater Interfaces*. 2018;10:26526.
- Zvagelsky RD, Chubich DA, Kolyagin DA, Korostylev EV, Kovalyuk VV, Prokhdotsov AI, Tarasov AV, Goltsman GN, Vitukhnovsky AG. *J Appl Phys*. 2020;53:355102.
- Xu Y, Gao B, He A, Zhang T, Zhang J. *Nanophotonics*. 2021;10:2110.
- Li KH, Fu WY, Cheung YF, Wong KKY, Wang Y, Lau KM, Choi HW. *Optica*. 2018;5:564.
- Sima F, Sugioka K, Vázquez RM, Osellame R, Kelemen L, Ormos P. *Nanophotonics*. 2018;7:613.
- Nocentini S, Martella D, Parmeggiani C, Wiersma DS. *Adv Opt Mater*. 2019;7:1900156.
- Krotkus S, Kasemann D, Lenk S, Leo K, Reineke S. *Light-Sci Appl*. 2016;5:e16121.

18. Catalano L, Karothu DP, Schramm S, Ahmed E, Rezgui R, Barber TJ, Famulari A, Naumov P. *Angew Chem.* 2018;57:17254.
19. Jiang L, Wu J, Li Q, Deng G, Zhang X, Li Z, Chen K, Chiang KS. *J Mater Chem C.* 2019;7:6257.
20. Wang C, Liu J, Zhang Z. *Opt Express.* 2022;30:31396.
21. Li H, Lin Z, Wang Y, An Z, Zhang S, Zhang Z, Tang C, Li E, Garcia J. *Opt Laser Technol.* 2022;153:108253.
22. Shi Q, Dong B, He T, Sun Z, Zhu J, Zhang Z, Lee C. *InfoMat.* 2020;2:1131.
23. Shabahang S, Kim S, Yun S. *Adv Funct Mater.* 2018;28:1706635.
24. Jiang N, Ahmed R, Rifat AA, Guo J, Yin Y, Montelongo Y, Butt H, Yetisen AK. *Adv Optical Mater.* 2018;6:1701118.
25. Liao C, Li C, Wang C, Wang Y, He J, Liu S, Bai Z, Gan Z, Wang Y. *Appl ACS. Mater Interfaces.* 2020;12:1465.
26. Lu G, Hong J, Qiu F, Spring AM, Kashino T, Oshima J, Ozawa M, Nawata H, Yokoyama S. *Nat Commun.* 2020;11:4224.
27. Messner A, Jud PA, Winiger J, Eppenberger M, Chelladurai D, Heni W, Baeuerle B, Koch U, Ma P, Haffner C, Xu H, Elder DL, Dalton LR, Smajic J, Leuthold J. *Nano Lett.* 2021;21:4539.
28. Zeng L, Pan Z, Xi X, Yang H, Ye Y, Huang L, Zhang H, Wang X, Wang Z, Zhou P, Xu X, Chen J. *Opt Lett.* 2021;46:1393.
29. Lim Y, Kwon OE, Kang S, Cho H, Lee J, Park Y, Cho N, Jin W, Lee J, Lee H, Kang J, Yoo S, Moon J, Bae B. *Adv Funct Mater.* 2018;28:1802944.
30. Liang J, Yan Y, Zhao Y. *Acc Mater Res.* 2021;2:340.
31. Song Y, Kim J, Cho H, Son Y, Lee M, Lee J, Choi K, Lee S. *ACS Nano.* 2020;14:1133.
32. Meng C, Chen E, Wang L, Tang S, Tseng M, Guo J, Ye Y, Yan Q, Kwok H. *Opt Express.* 2019;27:13098.
33. Gu C, Fei T, Lv Y, Feng T, Xue S, Lu D, Ma Y. *Adv Mater.* 2010;22:2702.
34. Zhang M, Xue S, Dong W, Wang Q, Fei T, Gu C, Ma Y. *Chem Commun.* 2010;46:3923.
35. Wang C, Zhang D, Zhang X, Wang J, Cheng R, Wang X, Yi Y, Sun X, Wang F, Chen C. *Appl Opt.* 2019;58:6820.
36. Zhang M, Zhang W, Wang F, Zhao D, Qu C, Wang X, Yi Y, Cassan E, Zhang D. *Sci Rep.* 2016;6:36729.
37. Zhang H, Zhang Y, Gu C, Ma Y. *Adv Energy Mater.* 2015;5:1402175.

Publisher's Note

Springer Nature remains neutral with regard to jurisdictional claims in published maps and institutional affiliations.

Submit your manuscript to a SpringerOpen[®] journal and benefit from:

- Convenient online submission
- Rigorous peer review
- Open access: articles freely available online
- High visibility within the field
- Retaining the copyright to your article

Submit your next manuscript at ► [springeropen.com](https://www.springeropen.com)
